L-H transition dynamics in fluid turbulence simulations with neoclassical force balance

L Chôné, P Beyer, Yanick Sarazin, G Fuhr, C Bourdelle, S Benkadda

L-H transition dynamics in fluid turbulence simulations with neoclassical force balance

L. Chôné,[1,2] P. Beyer,[1] Y. Sarazin,[2] G. Fuhr,[1] C. Bourdelle,[2] and S. Benkadda[1]
[1)] *Aix–Marseille Université, CNRS, PIIM UMR 7345, 13397 Marseille Cedex 20, France*
[2)] *CEA, IRFM, F-13108 Saint-Paul-lez-Durance, France.*

Spontaneous transport barrier generation at the edge of a magnetically confined plasma is reproduced in flux-driven three-dimensional fluid simulations of electrostatic turbulence. Here, the role on the radial electric field of collisional friction between trapped and passing particles is shown to be the key ingredient. Especially, accounting for the self-consistent and precise dependence of the friction term on the actual plasma temperature allows for the triggering of a transport barrier, provided the input power exceeds some threshold. In addition, the barrier is found to experience quasi-periodic relaxation events, reminiscent of Edge Localised Modes. These results put forward a possible key player, namely neoclassical physics via radial force balance, for the Low- to High-confinement regime transition observed in most of controlled fusion devices.

Regions of reduced energy and particle diffusion are observed in magnetic fusion devices such as tokamaks and stellarators[1,2]. These regions are named transport barriers and are equivalent to those observed in atmospheric and oceanic turbulent flows[3]. The high confinement mode or H-mode barrier, which forms at the edge of magnetic fusion devices was the earliest observed and the most studied[4]. Since then many theoretical models have been devoted to the study of this very promising confinement mode[2]. These theories share in common the fact that the potential structure that is observed in the H-mode regime, and which gives rise to a strong negative radial electric field, is indeed responsible for the turbulence suppression by shear effects in the $\mathbf{E}\times\mathbf{B}$ velocity at which fluctuations are convected[5]. On another hand, theory shows that the plasma gradients in the H-mode barrier are limited by pressure driven ballooning modes leading to relaxation oscillations of the barrier, known as Edge-Localized Modes (ELMs)[6]. These violent relaxation events bear similarities with solar flares[7]. The transition from a regime of low confinement to one of high confinement at the edge, or L-H transition occurs when externally injecting power into the plasma and is generally followed by quasi-periodic relaxations of the barrier, which is a characteristic of the ELMs. The importance of achieving high confinement makes H-mode one of the ITER baseline scenarios, however it could be seriously hindered by the harmful nature of ELMs to the wall components. Because of this, the understanding of the creation, control and removal of external transport barriers is of crucial importance to the success of magnetic fusion. Although the L-H transition has been widely observed and the conditions for triggering H-mode have been extensively studied experimentally, theoretical understanding of the underlying physical mechanisms remains unresolved[2,8–17]. In particular, although the self-generation of sheared flows and subsequent turbulence reduction is observed in the few flux-driven three-dimensional (3D) plasma edge turbulence simulations addressing this issue, no clear transition is reported[14–17]. When reported, such a transition is neither well characterised nor properly understood[18].

In this letter we present non-linear results of flux-driven resistive ballooning simulations of the plasma edge, taking into account the effect of neoclassical friction on the $\mathbf{E}\times\mathbf{B}$ flow. Such an effect has recently been explored in the frame of a 1D predator-prey model[19]. Here it is found by means of 3D simulations that competition between the neoclassical friction and zonal-flows (ZFs) allows for the existence of two distinct regimes depending on the imposed heat flux. These regimes correspond to a low-confinement state dominated by turbulence, and above a certain input power, a state of improved confinement with the onset of a transport barrier. In contrast to previous investigations, radial and temporal variations of the friction coefficients are retained. This feature is found to have a strong impact on the dynamics of the system, so that taking it into account is necessary to obtain generation of this transport barrier. A reduced 1D model which reproduces qualitatively the 3D result is derived, and 1D simulations show intermittent bursts of turbulent flux corresponding to relaxations of the established barrier.

In the following simulations, the non-linear evolution of electrostatic resistive ballooning turbulence is studied with the EMEDGE3D code[20] in toroidal geometry with circular, non-diverted poloidal cross-section. The dimensionless coordinates (x, y, z) of the 3D toroidal geometry refer to the minor radius, and the poloidal and toroidal angles, respectively. The code solves standard reduced MHD (RMHD) equations[20–23], in the limit of large aspect ratios and with the slab approximation:

$$\partial_t \nabla_\perp^2 \phi + \left\{\phi, \nabla_\perp^2 \phi\right\} = -\nabla_\parallel^2 \phi - \mathrm{G}p + \partial_x F_{neo} + \nu_\perp \nabla_\perp^4 \phi\,, \tag{1}$$

$$\partial_t p + \{\phi, p\} = \delta_c \mathrm{G}\phi + \chi_\parallel \nabla_\parallel^2 p + \chi_\perp \nabla_\perp^2 p + S\,. \tag{2}$$

Equations (1,2) correspond respectively to the charge and energy balance, the two fields ϕ and p being the electric potential and the total pressure. Poisson brackets $\{\phi,\cdot\} = \partial_x\phi\partial_y\cdot - \partial_y\phi\partial_x\cdot$ account for the advection

by the electric drift velocity. $\nabla_\parallel$ and$\nabla_\perp$ are respectively the parallel and perpendicular gradients with respect to the magnetic field lines and G is a toroidal curvature operator. $\nu_\perp$ is the classical viscosity, while $\chi_\parallel$ and $\chi_\perp$ account for parallel and perpendicular collisional heat diffusivities. $S(x)$ is a heat source term (all numerical results presented here are from flux-driven simulations). Here, the novel term in Eq. (1) is $\partial_x F_{neo}\left(\bar{\phi},\bar{p}\right)$, where $\bar{\phi}=\phi-\tilde{\phi}$ and $\bar{p}=p-\tilde{p}$ indicate flux-surface averaged quantities, with $\tilde{\phi}$ and $\tilde{p}$ the associated perturbations. It ensures that the poloidal flow relaxes towards its expected neoclassical value on collisional time, as a result of the friction between trapped and passing particles. The key steps for the derivation of F_{neo} are outlined in the following (for the full derivation, see[24]).

The system (1,2) is dimensionless: time is normalised to the interchange time, $\tau_{int}=\frac{\sqrt{R_0 L_p}}{\sqrt{2}c_{S0}}$, with $c_{S0}=\sqrt{p_0/n_0 m_i}$ the typical acoustic speed and L_p the typical pressure gradient length. The perpendicular length scale is the resistive ballooning length, $\xi_{bal}=\sqrt{\frac{\rho\eta_\parallel}{\tau_{int}}}\frac{L_s}{B_0}$, with the magnetic shear length L_s being the parallel length scale. The fields ϕ and p are normalised respectively to $\frac{B_0\xi_{bal}^2}{\tau_{int}}$ and $\frac{\xi_{bal}p_0}{L_p}$. Because the MHD model does not separate density and temperature, an assumption is made that the former is constant $n=n_0$, therefore $p_s=n_0T_s$. Furthermore, the ratio between ion and electron temperatures is kept constant $T_i=\epsilon_T T_e$.

The starting point of this reasoning is the radial force balance equation which, if we consider toroidal rotation to be negligible (generally true in the absence of torque injection), can be written thus:

$$\partial_x\bar{\phi}+\frac{\epsilon_T}{\epsilon_T+1}\frac{\tau_{int}p_0}{\xi_{bal}L_p e n_0 B_0}\partial_x\bar{p}=\bar{u}_y. \tag{3}$$

In the fluid model, the poloidal velocity is not normally constrained, however an expression emerges from the neoclassical theory: $\bar{u}_y^{neo}=\frac{\epsilon_T}{\epsilon_T+1}\frac{\tau_{int}p_0}{\xi_{bal}L_p e n_0 B_0}K\left(\nu_{i,*}\right)\partial_x\bar{p}$[25,26]. The collisionality is expressed as a function of $\bar{p}$ (since $\nu_{i,*}\propto nT_i^{-2}\propto\bar{p}^{-2}$, at constant density), and a heuristic closure[24] allows for this constraint to be taken into account in the fluid model through a friction term which enforces relaxation towards this equilibrium:

$$F_{neo}=-\mu_{neo}\left(\bar{p}\right)\left[\partial_x\bar{\phi}-K_{neo}\left(\bar{p}\right)\partial_x\bar{p}\right], \tag{4}$$

where $K_{neo}=\frac{\epsilon_T}{\epsilon_T+1}\frac{\tau_{int}p_0}{\xi_{bal}L_p e n_0 B_0}\left[K\left(\nu_{i,*}\right)-1\right]$, and $\mu_{neo}=\alpha_{neo}\mu_i\left[\frac{q(x)}{\varepsilon(x)}\right]^2$, with $q(x)$ the safety factor and $\varepsilon(x)$ the inverse aspect ratio. The Hinton and Hazeltine formula is used to determine $K\left(\nu_{i,*}\right)$ for all neoclassical regimes[25], and an approximate fit for μ_i is found in[24]. One can see in Eq.4 that alleviating the assumption of constant density would actually reinforce the coupling near the edge where n is small. For instance, under the assumption that $n\propto T$, the friction term in Eq.4 would have a similar structure with $\partial_x\bar{p}$ replaced by $\partial_x\bar{p}/\sqrt{\bar{p}}$. As a consequence, the neoclassical drive would be even stronger at the plasma edge.

Under the assumptions of the electrostatic RMHD model, ZF amplitude is likely overestimated. Indeed, the competition between Reynolds and Maxwell stresses is unaccounted for, and so is the saturation by collisional friction on the ZF (both effects are discussed in[28]). A factor $\alpha_{neo}>1$ is therefore introduced to recover the competition between zonal and neoclassical flows expected during the L-H transition (here $\alpha_{neo}=6$ is sufficient to achieve this). Note that the value of α_{neo} affects the magnitude of the transition threshold, but not the qualitative behaviour of the system. Importantly, two mechanisms can lead to sheared radial electric field here: on the one hand, pressure gradient and radial electric field get coupled, allowing for a possible positive feedback loop, and strong radial variations of K_{neo} will result in a sheared neoclassical flow on the other hand.

The simulations are carried out in the range of minor radius between $0.85<r/a<1$. This main simulation domain is bounded by buffer zones where the turbulence is artificially stabilised by large $\chi_\perp$ and $\nu_\perp$ coefficients. The precise value of $\chi_\perp$ in the buffer zones is chosen so as to maintain a gradient of order unity (in the buffers, $Q_0=Q_{coll}=-\chi_\perp\partial_x\bar{p}$). All simulations are flux-driven with a volume source $S(x)$ located in the $x<x_{in}$ buffer zone, imposing the heat flux $Q_0=\int S(x)\,dx$. Here x denotes the normalised minor radius (to ξ_{bal}), x_{in} and x_{out} are the positions of the main simulation domain's boundaries, with x_{out} corresponding to $r=a$. The safety factor is hyperbolic, between $q(x_{in})=2.5$ and $q(x_{out})=3.5$. The set of parameters used here is representative of medium to large present tokamaks. In particular, collisionality is in the range $10^{-1}<\nu_{i,*}<10^2$ (near banana to collisional regime), which is in agreement with what is observed in L-mode at the edge[27], and happens to be where $K\left(\nu_{i,*}\right)$ varies the most rapidly. This is with the exception of $\nu_\perp$ and $\chi_\perp$, chosen large enough to ensure damping at sub-Larmor scales. Here we take $\chi_\perp=\nu_\perp=0.93$ and $\chi_\parallel=2$ (these values are normalised to ξ_{bal}^2/τ_{int} in the perpendicular direction and L_s^2/τ_{int} in the parallel direction). Several simulations are done in the range of $5\leq Q_0\leq 30$ to study the impact of this friction on confinement.

The results on figure 1 show the confinement deterioration expected in L-mode with increasing heat flux for $Q_0<14$, followed by a sharp increase and again a deterioration if the source is increased further. This corresponds to strong changes in the profiles of the flux-surface averaged pressure and poloidal component of the drift velocity $\bar{u}_{Ey}=\partial_x\bar{\phi}$. Indeed, when the heat flux is below $Q_0=14$, the pressure profile is roughly a straight line and the poloidal velocity is low with minor radial corrugations. Above the threshold, the poloidal velocity profile is strongly modified. In the main part of the simulation domain it stays at low amplitude and changes sign, but between $0.95<r/a<1$ it peaks strongly, generating a

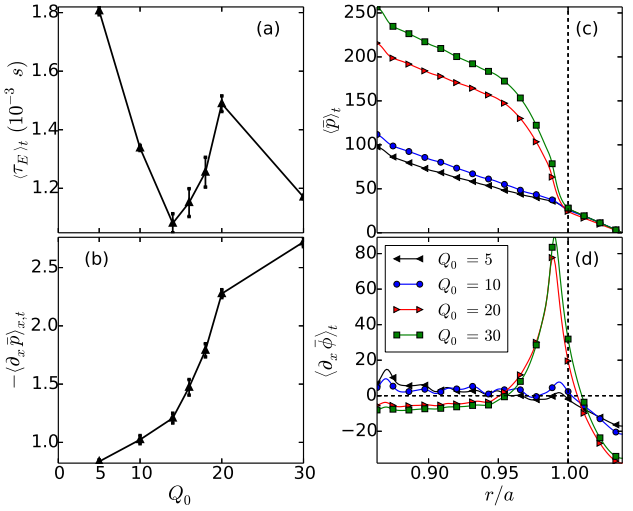

FIG. 1. (Color online). Evolution of the mean energy confinement time (a), defined as $\tau_E = 1/Q_0 \int_{x_{in}}^{x_{out}} \bar{p}\, dx$, and the volume-averaged mean pressure gradient (b) as functions of the heat source amplitude in the 3D case. Error bars on (a) and (b) show the standard deviation in time. (c) and (d) show mean profiles of the pressure and the $\mathbf{E} \times \mathbf{B}$ velocity. The vertical dashed lines on (c) and (d) mark the LCFS. All time-averaged quantities are taken over a statistically stationary period of the order of $1000\,\tau_{int}$.

localised sheared flow. Note that throughout the domain below the threshold and outside the barrier above, the turbulent flux is one order of magnitude larger than the collisional flux. The stabilising effect of sheared flows on turbulence, which is a well documented result from reduced models to gyrokinetic simulations[12,14,29–31], allows for steeper pressure gradients to be reached, giving a pedestal-like pressure profile. In the higher range of heat flux, the poloidal velocity tends towards the force-balance value, $\bar{u}_{Ey} = K_{neo}\partial_x \bar{p}$, while it departs from it for the lower sources. Furthermore, the shape of the velocity profile shows good qualitative agreement with measurements of the radial electric field in H-mode[32–34], even though the radial electric field at the last closed field-surface (LCFS) is not constrained by scrape-off layer physics in the model (i.e. E_r is allowed to vary freely inside the buffer zones. Notice however that E_r becomes positive in the outer buffer region, as expected in the SOL). We also show that the mean value of the poloidal velocity at the peak, and consequently the associated shear, is significantly increased (here about 3 times larger) when K_{neo} and its radial variations are taken into account (see Fig. 2). Correspondingly, the friction coefficients, as calculated from the equilibrium pressure in the code, show large changes before and after the transition. In particular, as shown on Fig. 3 (left panel) the maximum value of K goes from -1 for $Q_0 < 14$ (transition from collisional to plateau neoclassical regime) to 0 (plateau regime) after the transition. Moreover, after the transition the profile of K is ranging from -2.1 to 0 with a strong gradient at the position of the barrier. Correspondingly, the value of μ_{neo} doubles at the position of the barrier after the transition (as illustrated in Fig. 3, right panel), and shows a very sharp gradient outward from this position. This supports the fact that the radial and temporal variations of both coefficients should be taken into account, K in order to allow for strong enough shear flows, and μ_{neo} in order to allow for competition between neoclassical friction and ZF.

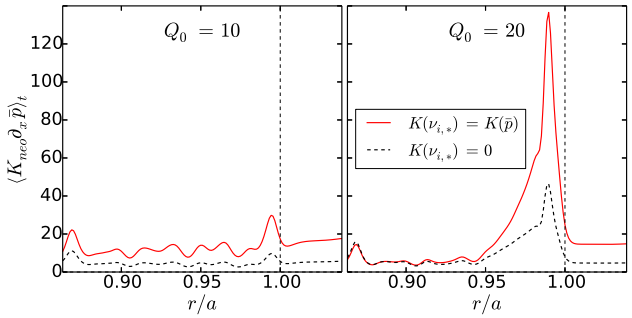

FIG. 2. (Color online). Comparison of the friction-imposed drift velocity $\bar{u}_{Ey} = K_{neo}\partial_x \bar{p}$ with $K(\nu_{i,*}) = 0$ and $K(\nu_{i,*}) = K(\bar{p})$, in the lower and higher range of heat flux.This illustrates that the barrier could not form or maintain itself if the radial and temporal variations of K where not taken into account.

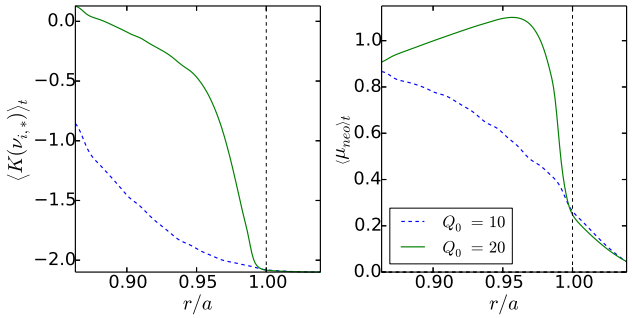

FIG. 3. (Color online). Profiles of $K(\nu_{i,*})$ and μ_{neo} shown for two values of input power, before and after the transition.

Smooth approach of the threshold has shown dithering of the poloidal velocity, reminiscent of the I-phase in slow L-H transitions[35–40]. This is clearly seen when looking at the time evolution of the poloidal velocity and the associated shearing rate, as shown on Fig. 4. Before the formation of the transport barrier the normalised velocity shear fluctuates in between 1 and 2 . An increase to twice this value is then observed shortly after 1 ms, soon followed by a sharp fall back to its original level. This is repeated twice, each time towards higher velocities, before a new state is reached at $t > 2$ ms and a barrier is established. As can be seen on the lower panel of Fig. 4, the radial maximum of the velocity corresponds to the peak observed in Fig. 1d in the case of a steady barrier.

It is instructive to realise that similar characteris-

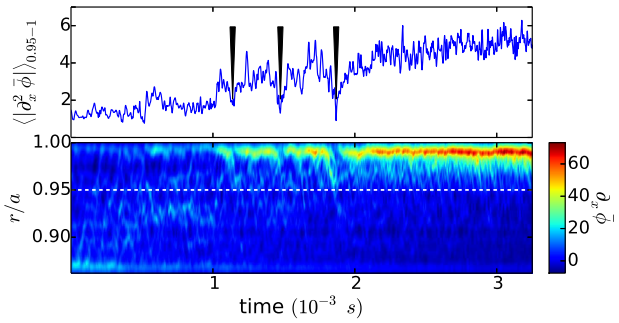

FIG. 4. (Color online). Time evolution of the poloidal velocity when crossing slowly the threshold. Upper panel shows evolution of the average shearing rate in the range $0.95 \leq r/a \leq 1$, with black wedges pointing at the repeated drops during the transition. Lower panel time evolution of the poloidal velocity radial profile, with the white dashed line highlighting the position $r/a = 0.95$. Here the statistically stationary phase is not shown.

tics can be obtained with a reduced 1D model, provided neoclassical friction is properly accounted for. This model derives from Eqs. 1-2, when only retaining resonant modes, characterised by $k_\parallel = 0$, and one single poloidal mode of wave vector k. Then, p and ϕ can be decomposed into their equilibrium and fluctuating parts: $f = \bar{f} + \tilde{f}e^{\imath ky} + \text{c.c.}$, with $f = (p, \phi)$. The following four-fields 1D system is obtained[41]:

$$\partial_t \bar{p} = -\imath k \partial_x \left(\tilde{p}\tilde{\phi}^* - \tilde{p}^*\tilde{\phi}\right) + \chi_\perp \partial_x^2 \bar{p} + S(x), \quad (5)$$

$$\partial_t \bar{u}_{Ey} = \imath k \partial_x \left(\tilde{\phi}\partial_x\tilde{\phi}^* - \tilde{\phi}^*\partial_x\tilde{\phi}\right) - \mu_{neo}\left(\bar{u}_{Ey} - K_{neo}\partial_x\bar{p}\right) + \nu_\perp \partial_x^2 \bar{u}_{Ey}, \quad (6)$$

$$\partial_t \tilde{p} = \imath k \left[\tilde{\phi}\left(\partial_x\bar{p} - \kappa\right) - \bar{u}_{Ey}\tilde{p}\right] - \alpha_p|\tilde{p}|^2\tilde{p} + \chi_\perp\partial_x^2\tilde{p}, \quad (7)$$

$$\partial_t \tilde{\phi} = \imath\left(\frac{g}{k}\frac{\tilde{p}}{\bar{p}} - k\bar{u}_{Ey}\tilde{\phi}\right) - \alpha_\phi|\tilde{\phi}|^2\tilde{\phi} + \nu_\perp\partial_x^2\tilde{\phi}, \quad (8)$$

The $\alpha_f|\tilde{f}|^2\tilde{f}$ terms account for saturation via mode coupling. Here t is normalised to $\frac{1}{\omega_S} = \frac{m_i}{eB_0}$, x to $\rho_S = \frac{\sqrt{m_i k_B T_e}}{eB_0}$.

In this case, partial stabilisation of the turbulence is achieved above a certain threshold of the injected power, as illustrated on Fig. 5, showing that this reduced model still contains the minimal elements to reproduce this behaviour. In the parameter range considered so far, it turns out that for low fluxes, the collisional and turbulent fluxes are of the same order of magnitude (Fig. 5, right panel). This 1D model offers the advantage of allowing for long simulation runs, on several energy confinement times. Especially, when the input power exceeds the L-H transition threshold, a complex dynamics emerges: here turbulence is not steadily suppressed but shows instead quasi-periodic bursts. Interestingly the pseudo-period increases with the injected power (see Fig. 6). This behaviour bears similarities with type-III ELMs, which were already suggested to be governed by the resistive ballooning instability[16,20,30,42,43].

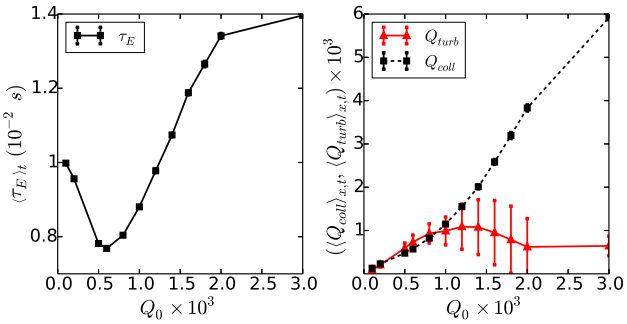

FIG. 5. (Color online). Evolution of the confinement efficiency as a function of the heat source amplitude in the 1D case.

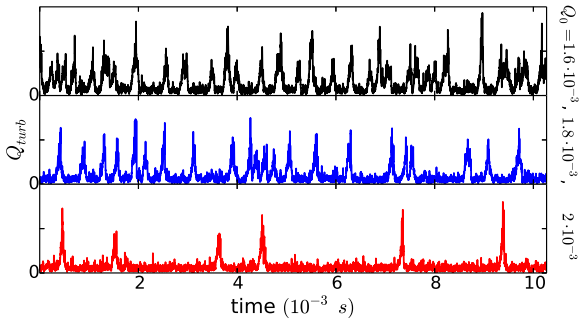

FIG. 6. (Color online). Time evolution of the turbulent flux in the presence of a barrier for different input powers, in the 1D case. The panels are in order of increasing power.

In conclusion, 3D nonlinear simulations of flux-driven edge turbulence are performed in a fluid model including neoclassical friction via a heuristic closure. They have shown the existence of two distinct regimes of confinement depending on the imposed heat flux. The transition scenario from one regime to another is the following: increasing the input power leads to more violent avalanches, triggering strong stabilising ZF. The resulting steepening of the pressure gradient further generates a sheared mean flow via the neoclassical friction. If the shear becomes strong enough to prevent a new burst, the barrier locks on because of this positive feedback loop between pressure gradient and poloidal flow, mediated by neoclassical terms. If not, it collapses in a strong transport event, starting another similar cycle. This can be repeated before the transition, resembling limit cycle oscillations observed in L-I-H transition experiments[35–40]. The stability of this barrier over long periods has been explored by means of a reduced 1D model, which reproduces the general behaviour of the 3D model, and revealed the existence of relaxations reminiscent of type-III ELMs.

The authors thank X. Garbet, Y. Camenen and D. F. Escande for fruitful discussions and insightful ad-

vices. This work is supported by the French National Research Agency, project ANR-2010-BLAN-940-01. Computations have been performed at the Mésocentre d'Aix-Marseille Université. This work, supported by the European Communities under the contract of Association between Euratom and CEA, was carried out within the framework of the European Fusion Development Agreement. The views and opinions expressed herein do not necessarily reflect those of the European Commission.

[1]G. M. Staebler, Plasma Phys. Control. Fusion **40** (1998) 569.
[2]J. W. Connor and H. R. Wilson, Plasma Phys. Control. Fusion **42** (2000) R1–R74.
[3]J. G. Esler, Phys. Fluids **20** (2008) 116602.
[4]F. Wagner, G. Becker, K. Behringer, D. Campbell, A. Eberhagen, W. Engelhardt, G. Fussman, O. Gehre, J. Gernhardt, G. v. Gierke, G. Haas, M. Huang, F. Karger, M. Keilhacker, O. Klüber, M. Kornherr, K. Lackner, G. Lisitano, G. G. Lister, H. M. Mayer, D. Meisel, E. R. Müller, H. Murmann, H. Niedermeyer, W. Poschenrieder, H. Rapp, H. Röhr, F. Schneider, G. Siller, E. Speth, A. Stäbler, K. H. Steuer, G. Venus, O. Vollmer, and Z. Yü, Phys. Rev. Lett. **49**, 1408 (1982).
[5]K. Itoh and S.-I. Itoh, Plasma Phys. Control. Fusion **38**, 1 (1996).
[6]H. R. Wilson, S. C. Cowley, A. Kirk, P. B. Snyder, Plasma Phys. Control. Fusion **48**, (2006) A71–A84.
[7]W. Fundamenski, V. Naulin, T. Neukirch, O. E. Garcia and J. Juul Rasmussen, Plasma Phys. Control. Fusion **49** (2007) R43.
[8]S.-I. Itoh, K. Itoh, Phys. Rev. Lett. **60**, 2276 (1988).
[9]B. A. Carreras, D. Newman, P. H. Diamond, Y. M. Lang, Phys. Plasmas **1**, 4014 (1994).
[10]E. Kim and P. H. Diamond, Phys. Plasmas **10**, 1698 (2003).
[11]P. N. Guzdar, R. G. Kleva, R. J. Groebner, and P. Gohil, Phys. Plasmas **11**, 1109 (2004).
[12]M. A. Malkov and P. H. Diamond, Phys. Plasmas **15**, 122301 (2008).
[13]W. Fundamenski, F. Militello, D. Moulton and D. C. McDonald, Nucl. Fusion **52** (2012) 062003.
[14]F. L. Hinton and G. M. Staebler, Phys. Fluids B **5**, 1291 (1993).
[15]J. F. Drake, Y. T. Lau, P. N. Guzdar, A. B. Hassam, S. V. Novakovski, B. Rogers, and A. Zeiler, Phys. Rev. Lett. **77**, 494 (1996).
[16]P. Beyer, S. Benkadda, G. Fuhr-Chaudier, X. Garbet, Ph. Ghendrih and Y. Sarazin, Plasma Phys. Control. Fusion **49** (2007) 507–523.
[17]A. Thyagaraja, M. Valovič, and P. J. Knight, Phys. Plasmas **17**, 042507 (2010).
[18]X. Q. Xu, R. H. Cohen, T. D. Rognlien, and J. R. Myra, Phys. Plasmas **7**, 1951 (2000).
[19]K. Miki, P. H. Diamond, Ö. D. Gürcan, G. R. Tynan, T. Estrada, L. Schmitz, and G. S. Xu, Phys. Plasmas **19**, 092306 (2012).
[20]G. Fuhr, P. Beyer, S. Benkadda, and X. Garbet, Phys. Rev. Lett. **101**, 195001 (2008).
[21]R. D. Hazeltine, M. Kotschenreuther, and P. J. Morrison, Phys. Fluids **28**, 2466 (1985).
[22]A. Zeiler, D. Biskamp, J. F. Drake, and B. N. Rogers, Phys. Plasmas **5**, 2654 (1998).
[23]P. Beyer, S. Benkadda, X. Garbet, and P. H. Diamond, Phys. Rev. Lett. **85**, 4892 (2000).
[24]T. A. Gianakon, S. E. Kruger, and C. C. Hegna, Phys. Plasmas **9**, 536 (2002).
[25]F. L. Hinton and R. D. Hazeltine, Rev. Mod. Phys. **48**, 239 (1976).
[26]P. Helander and D. J. Sigmar, Collisional Transport in Magnetized Plasmas, Cambridge University Press (2005).
[27]C. Bourdelle, X. Garbet, R. Singh, and L. Schmitz, Plasma Phys. Control. Fusion **54** (2012) 115003.
[28]P. H. Diamond, S.-I. Itoh, K. Itoh, and T. S. Hahm, Plasma Phys. Control. Fusion **47** (2005) R35–R161.
[29]H. Biglari, P. H. Diamond, and P. W. Terry, Phys. Fluids B **2**, 1 (1990).
[30]P. Beyer, S. Benkadda, G. Fuhr-Chaudier, X. Garbet, Ph. Ghendrih, and Y. Sarazin, Phys. Rev. Lett. **94**, 105001 (2005).
[31]A. Strugarek, Y. Sarazin, D. Zarzoso, J. Abiteboul, A. S. Brun, T. Cartier-Michaud, G. Dif-Pradalier, X. Garbet, Ph. Ghendrih, V. Grandgirard, G. Latu, C. Passeron, and O. Thomine, Plasma Phys. Control. Fusion **55** (2013) 074013.
[32]P. Sauter, T. Pütterich, F. Ryter, E. Viezzer, E. Wolfrum, G. D. Conway, R. Fischer, B. Kurzan, R. M. McDermott, S. K. Rathgeber and the ASDEX Upgrade Team, Nucl. Fusion **52** (2012) 012001.
[33]E. Wolfrum, P. Sauter, M. Willensdorfer, F. Ryter, F. Aumayr, L. Barrera–Orte, A. Burckhart, E. Fable, R. Fischer, B. Kurzan, T. Pütterich, S. K. Rathgeber, W. Suttrop, E. Viezzer and the ASDEX Upgrade Team, Plasma Phys. Control. Fusion **54** (2012) 124002.
[34]E. Viezzer, T. Pütterich, G. D. Conway, R. Dux, T. Happel, J. C. Fuchs, R. M. McDermott, F. Ryter, B. Sieglin, W. Suttrop, M. Willensdorfer, E. Wolfrum and the ASDEX Upgrade Team, Nucl. Fusion **53** (2013) 053005.
[35]H. Zohm, ASDEX-Upgrade Team, and NI and ICRH Group, Phys. Rev. Lett. **72**, 222 (1994).
[36]R. J. Colchin, M. J. Schaffer, B. A. Carreras, G. R. McKee, R. Maingi, T. N. Carlstrom, D. L. Rudakov, C. M. Greenfield, T. L. Rhodes, E. J. Doyle, N. H. Brooks, and M. E. Austin, Phys. Rev. Lett. **88**, 255002 (2002).
[37]L. Schmitz, L. Zeng, T. L. Rhodes, J. C. Hillesheim, E. J. Doyle, R. J. Groebner, W. A. Peebles, K. H. Burrel, and G. Wang, Phys. Rev. Lett. **108**, 155002 (2012).
[38]J. Cheng, J. Q. Dong, K. Itoh, L. W. Yan, M. Xu, K. J. Zhao, W. Y. Hong, Z. H. Huang, X. Q. Ji, W. L. Zhong, D. L. Yu, S.-I. Itoh, L. Nie, D. F. Kong, T. Lan, A. D. Liu, X. L. Zou, Q. W. Yang, X. T. Ding, X. R. Duan, Yong Liu, and the HL-2A Team, Phys. Rev. Lett. **110**, 265002 (2013).
[39]T. Kobayashi, K. Itoh, T. Ido, K. Kamiya, S.-I. Itoh, Y. Miura, Y. Nagashima, A. Fujisawa, S. Inagaki, K. Ida, and K. Hoshino, Phys. Rev. Lett. **111**, 035002 (2013).
[40]G. S. Xu, L. M. Shao, S. C. Liu, H. Q. Wang, B. N. Wan, H. Y. Guo, P. H. Diamond, G. R. Tynan, M. Xu, S. J. Zweben, V. Naulin, A. H. Nielsen, J. Juul Rasmussen, N. Fedorczak, P. Manz, K. Miki, N. Yan, R. Chen, B. Cao, L. Chen, L. Wang, W. Zhang, and X. Z. Gong, Nucl. Fusion **54** (2014) 013007.
[41]S. Benkadda, P. Beyer, N. Bian, C. Figarella, O. Garcia, X. Garbet, P. Ghendrih, Y. Sarazin, and P. H. Diamond, Nucl. Fusion **41** (2001) 995.
[42]J. W. Connor, Plasma Phys. Control. Fusion **40** (1998) 531–542.
[43]W. Suttrop, Plasma Phys. Control. Fusion **42** (2000) A1–A14.